JOURNAL OF SOLID STATE CHEMISTRY 119, 271–280 (1995)

Properties of $LaCo_{1-t}Cr_tO_3$

II. Reduction and Reoxidation

B. Gilbu Tilset, H. Fjellvåg, and A. Kjekshus[1]

Department of Chemistry, University of Oslo, P.O. Box 1033 Blindern, N-0315 Oslo, Norway

Received February 16, 1995; accepted May 11, 1995

The reduction and reoxidation properties of the $LaCo_{1-t}Cr_tO_{3-\delta}$ solid-solution series have been studied by TPD, TPR, PXD, TGA, and XPS. At moderate temperatures, reduction by hydrogen removes oxygen from $LaCo_{1-t}Cr_tO_3$ in a topotactic process which converts Co^{III} to Co^{II}. Bulk Cr^{III} is not affected; hence $LaCo_{1-t}Cr_tO_{3-(1-t)/2}$ is the borderline composition of the reduced state. TPR shows that the reduction occurs in several steps, indicating that different reaction mechanisms are involved. Surface reduction, confirmed by XPS for the Cr-rich samples, is one such process. The as-prepared samples contain higher-valent (>III) chromium surface species, the concentration of which is significantly decreased upon the reductive treatment. The reduction and subsequent reoxidation processes are reversible, and reduced samples with $t < 0.60$ are unstable with respect to reoxidation even at ambient. The unit-cell volume per formula unit of $LaCo_{1-t}Cr_tO_{3-\delta}$ increases upon reduction, and indications of vacancy ordering are found for the Co-rich samples, where $La_2Co_2O_5$ is the reduced end state.

1. INTRODUCTION

The end members of the solid-solution series $LaCo_{1-t}Cr_tO_3$ differ widely with respect to reactions under reducing atmospheres. $LaCoO_3$ is easily reduced and is one of the perovskite-type oxides that can undergo topotactic, low-temperature reduction to vacancy-ordered phases according to the formal reaction (1–4)

$$2ABO_3(s) \rightarrow A_2B_2O_5(s) + \tfrac{1}{2}O_2(g).$$

Six different structure types have been reported (5) for the resulting $A_2B_2O_5$ phases. The orthorhombic brownmillerite-type structure has been found for $La_2Co_2O_5$ (4). This structure is related to the perovskite type and is characterized by planes of Co in tetrahedral sites alternating with planes of Co in octahedral coordination. $LaCrO_3$, on the other hand, is quite stable in reducing atmospheres at low as well as high temperatures (6, 7).

The present study concerns the compositional variation of redox properties for $LaCo_{1-t}Cr_tO_3$. This is part of a program aimed at exploring correlations between physical and chemical properties of perovskite-type oxides and their catalytic activity with respect to CO oxidation. A redox process in the surface region of the catalyst is believed to play a central role in this reaction.

The phase changes which occur upon sample reduction are considered in relation to the findings reported in paper I (8) of this series, which concerns the solid solubility, thermal expansion, and structural transition of fully oxidized $LaCo_{1-t}Cr_tO_3$.

2. EXPERIMENTAL

The samples of $LaCo_{1-t}Cr_tO_3$ were prepared by multiple firing of citrate gels, as described previously (8). The starting materials were La_2O_3 (99.98%, Fluka or 99.99%, Molycorp), $Co(CH_3COO)_2 \cdot 4H_2O$ (>99.0%, Fluka), CrO_3 (>99%, Merck) and $C_3H_4(OH)(COOH)_3 \cdot H_2O$ (reagent grade, Sturge Biochemicals). Prior to use, La_2O_3 was heated to 1273 K in air to remove hydrated and/or carbonated species, and the metal contents of the cobalt acetate and the chromium oxide were determined thermogravimetrically. The final calcination was performed at 1073 K (1173 K for $t = 0.40$ and 1.00), with slow cooling (1 K min^{-1}) to room temperature.

All samples were checked for purity and characterized by powder X-ray diffraction (PXD) in the as-prepared state, after reduction, and after reoxidation. Guinier–Hägg cameras were used, with $CrK\alpha_1$ radiation and Si as internal standard. All PXD photographs were evaluated manually, using a comparator. Unit-cell parameters were calculated using the CELLKANT program (9).

Freshly reduced samples (with $t = 0.10$, 0.20, 0.30, 0.40, 0.50, and 0.85) were obtained by treatment in 10% H_2 in N_2 at 733 K (in accord with TPR results, Sec. 3.1),

[1] To whom correspondence should be addressed.

0022-4596/95 $12.00

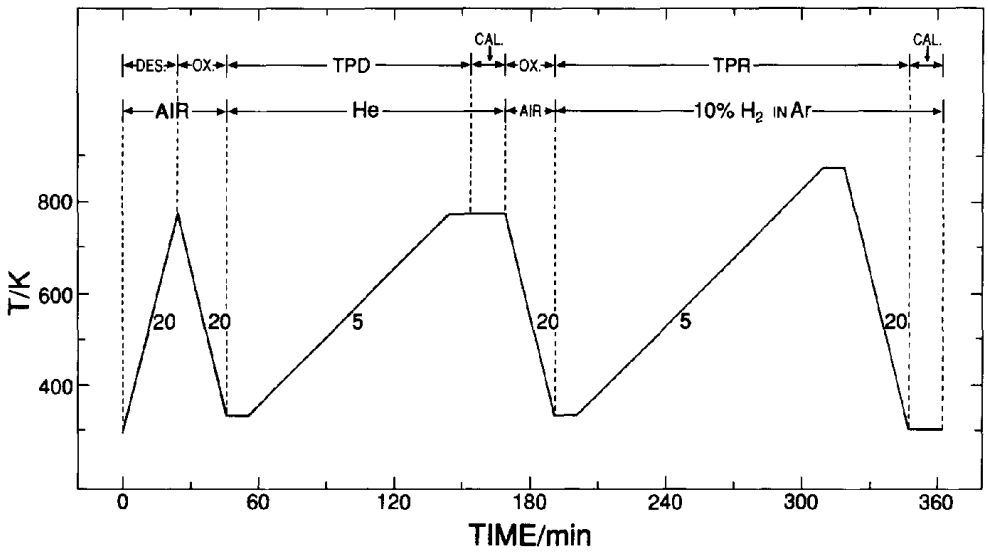

FIG. 1. Programmed variations during TPD/TPR runs. Heating and cooling rates are given in K min^{-1}. DES.: desorption of surface contaminants, like water or carbonates; OX.: sample oxygenation; CAL.: TCD calibration. Actual cooling rates were appreciably lower than those programmed.

cooled to room temperature in the reducing atmosphere, and studied by PXD within 4 hr of exposure to ambient conditions.

Surface areas were measured using a Quantachrome Monosorb single-point BET apparatus, with nitrogen as adsorbent.

Temperature programmed desorption (TPD) and reduction (TPR) were performed for t = 0.00, 0.20, 0.40, 0.60, 0.70, 0.80, 0.90, 0.95, and 1.00 using an AMI-1 Catalyst Characterization System from Altamira Instruments, with a thermal conductivity detector (TCD) for monitoring changes in the oxygen or hydrogen concentrations.

For the TPD and TPR experiments, the powder samples were first pressed into pellets, then coarsely crushed and sifted. The 0.2 to 0.8 g of the particle-size fraction obtained between the sieves of mesh 35 (0.500 mm) and 70 (0.210 mm) was investigated in each TPD/TPR experiment; experiments were programmed according to the scheme shown in Fig. 1. For t = 0.00, the maximum temperatures for TPR were 703 or 773 K and for t = 0.95, 923 K. Due to limitations of the cooling system, actual cooling rates were appreciably lower than those programmed, especially at the lowest temperatures. After TPD/TPR, the reaction cell was opened (at 303 K), and the reduced samples were stored at ambient temperature. PXD was performed within two weeks of reduction.

Instrument calibration was performed by reducing stoichiometric $LaCoO_3$ to La_2O_3 and Co (heating rate 5 K min^{-1}, T_{max} 1173 K). The resulting phase composition of the sample was confirmed by PXD.

In selected TPR experiments (t = 0.00, 0.90, and 0.95), the effluent gases were analyzed by mass spectroscopy (MS) for m/e ratios: 2, 15, 16, 17, 18, 28, 29, 30, 32, 40, 44, and 45, using a VG Quadrupoles Sensorlab instrument with Sensorlab 200D Quasar V6-2 software.

Reoxidation in air was studied by thermogravimetric analysis (TGA) within 2 weeks after the TPR measurements, using a Perkin–Elmer, 7 Series Thermal Analysis System (TGA7, heating rate: 5 K min^{-1}). Reoxidation of one $LaCoO_{3-\delta}$ sample was performed on a Stanton Redcroft STA 785 TG/DSC instrument within 1 hr of sample reduction, with PXD performed simultaneously.

Surface analyses were performed by X-ray photoelectron spectroscopy (XPS), using a VG Microlab III XPS/SAM instrument with Mg$K\alpha$ radiation. Samples were as-prepared powders with t = 0.00, 0,20, 0.40, 0.60, 0.80, and 1.00, and t = 0.80 and 1.00 reduced by TPR (and stored at ambient for more than a month). The samples were attached to the sample holder with Scotch tape. Analyses of the spectra were performed by the least-squares method for peak synthesis inherent to the VG instrumentation. All spectra were treated in the same manner, considering three oxygen peaks and two peaks for each of lanthanum, chromium, and cobalt. Fitted variables were peak position, full width at half maximum (FWHM), peak height, and peak shape (given as % Gaussian vs Lorentzian). Peak positions are referred to C 1s at 284.6 eV. Concentrations of different species were calculated on the basis of the integrated peak areas determined during peak synthesis. Contributions from surface carbon were disregarded and the concentrations of metals and oxygen were normalized using tabulated photoelectron

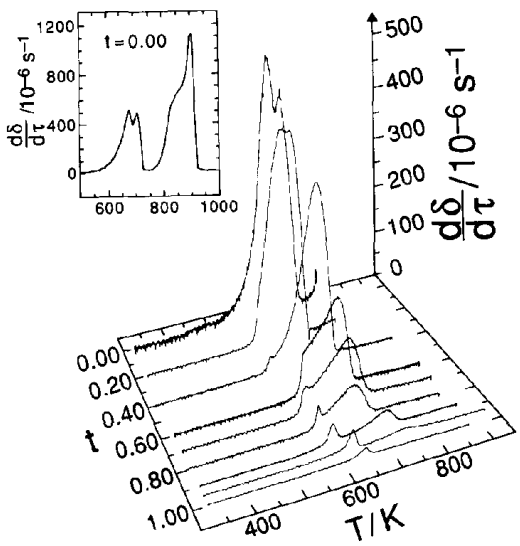

FIG. 2. TPR curves for reduction of $LaCo_{1-t}Cr_tO_3$ to $LaCo_{1-t}Cr_tO_{3-\delta}$, heating rate: 5 K min^{-1}, reduction rate in $d\delta/d\tau$. Inset shows the complete TPR curve for $LaCoO_3$ (viz. reduction to La_2O_3 and Co).

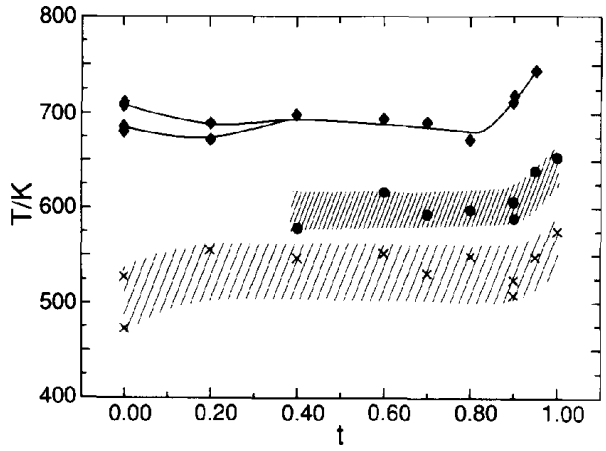

FIG. 3. Characteristic temperatures in TPR profiles for reduction of $LaCo_{1-t}Cr_tO_3$, heating rate: 5 K min^{-1}. × denotes the start of reduction, ● the low-temperature peak, and ◆ the high-temperature peak(s).

cross sections relative to C 1*s* (10). This will not necessarily give accurate concentration values, but will allow one to recognize trends. For $LaCrO_3$, XPS was performed before and after sputtering with Ar^+ for 1 hr, which corresponds to a sputtering depth of 10 to 30 nm.

3. RESULTS

3.1. Desorption and Reduction Studies by TPD and TPR

None of the studied samples showed reproducible oxygen desorption during TPD measurements. However, out of three $LaCoO_3$ samples examined, one showed possible oxygen desorption between 570 and 770 K, quantified to about half a surface layer of oxygen. Thus, if occurring at all, desorption involves only minute amounts of the desorbing species.

In the TPR plots shown in Fig. 2, the signal has been converted to express the rate of oxygen removal per mole sample. Parallel TPR measurements for $t = 0.00$ (five samples) and 0.90 (two samples) showed good reproducibility, with respect to both the peak profile and the amount of hydrogen reacted per mole sample. However, when the heating rate was lowered from 5 to 1 K min^{-1}, a 40 K shift of the peaks for $LaCoO_3$ toward lower temperatures was observed.

Figure 3 shows the temperature for the start of the reduction, along with peak temperatures for the different "reduction steps," obtained with a heating rate of 5 K min^{-1}. The uncertainty in the individual temperatures is estimated to be ±10 K. For $t = 0.00$ and 0.90, data from two separate TPR runs are plotted. The reproducibility appears to be better for the high than the low temperature reduction processes. Surface areas were almost constant, in the range from 1.5 to 3.3 $m^2\,g^{-1}$, for all samples investigated (t = 0.00, 0.20, 0.40, 0.60, 0.70, 0.80, 0.90, and 1.00). Thus, varying surface area is not likely to be the root of the different reactivities.

The TPR plot for the total reduction of $LaCoO_3$ to La_2O_3 and Co is shown in the inset to Fig. 2. The final reduction step starts at around 750 K for $LaCoO_3$, but this step is not included among the results considered in Fig. 3.

The amount of oxygen removed prior to the final reduction step is expressed as δ in the formula $LaCo_{1-t}Cr_tO_{3-\delta}$. As seen from Fig. 4, there is a linear relationship between δ and t: $\delta = 0.500 \cdot (1 - t)$. The amount of oxygen removed

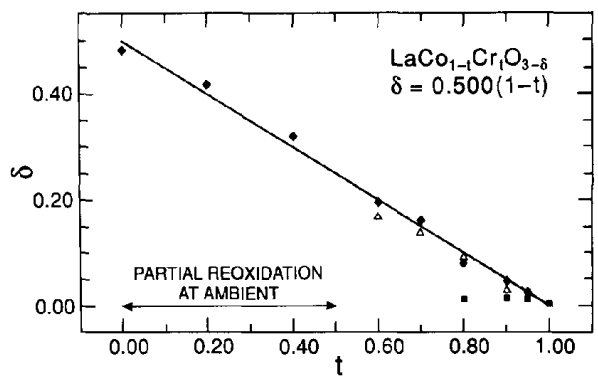

FIG. 4. Compositional dependence of oxygen nonstoichiometry, expressed as δ in $LaCo_{1-t}Cr_tO_{3-\delta}$ after TPR. ◆ refers to overall δ from TPR, ■ to the contribution to δ from the low-temperature TPR peak, and △ to overall δ according to TGA for reoxidation. Estimated error limits in δ, based on repeated TPR measurements, varies from ~0.03 for t = 0.00 to ~0.01 for t = 0.90.

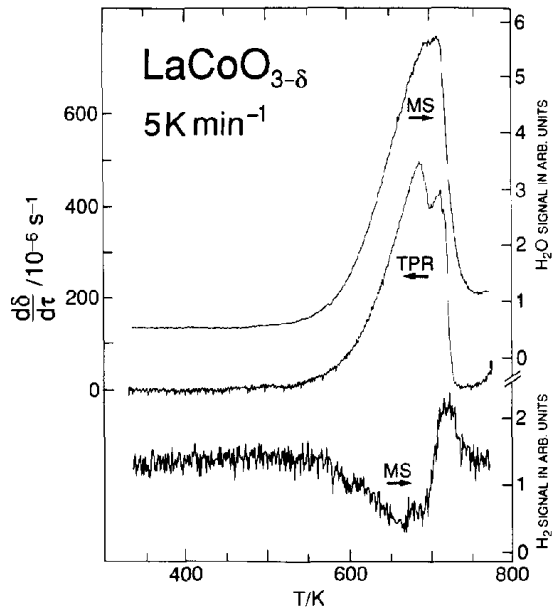

FIG. 5. Comparison of TPR and MS scans for reduction of $LaCoO_3$ to $LaCoO_{3-\delta}$.

in the first, rather small reduction step, cf. Fig. 2, is marked separately in Fig. 4 for $t \geq 0.80$.

3.2. MS of Effluent Gases

Attempts were made to detect species possibly desorbed during TPD by MS, which was considered to be more sensitive to small changes in gas concentrations than TCD. Indeed, MS showed desorption above 520 K; the first species detected were hydrocarbons and oxygen, and as the amount of hydrocarbons decreased, CO_2 was evolved. The latter species probably result from reactions involving hydrocarbons and oxygen adsorbed on the sample surface. However, the amounts of these gases were very small, and no desorption was detected by TCD. Also during the TPR experiments, traces of carbon-containing species were detected, even for $t = 0.00$ when TPD had been performed prior to TPR. It was considered pointless to ascertain the origin of these species, although it is likely that they are introduced as trace impurities in the flow gases, and, hence, are not an intrinsic part of the current research problem.

MS data for H_2 and H_2O are shown together with the corresponding TPR plot for $LaCoO_3$ in Fig. 5. The MS data for hydrogen consumption and water generation match the H_2 consumption as detected by TPR. The blurring of the peak profiles generally observed in the MS data probably reflects the diffusion process in the gas phase during the transport from the reaction cell to the MS detector. For $LaCoO_3$ run at 1 K min^{-1}, the MS peak profile is more distinct and similar to that found by TPR.

3.3. TGA of the Reoxidation Process

The amount of oxygen taken up during sample reoxidation in the TGA apparatus is included in Fig. 4 for samples with $t \geq 0.60$. The results are in agreement with reduction data obtained by TPR. For samples with larger Co contents, partial reoxidation occurs when the samples are exposed to air at ambient. For the reduced end phase, $LaCoO_{2.5}$, reoxidation occurs instantly and is distinctly exothermal. TGA performed after 1 hr at ambient conditions showed that $LaCoO_{2.5}$ had already been reoxidized to $LaCoO_{2.69}$. For $LaCoO_{2.5}$, total reoxidation to $\delta = 0.00$ at ambient is merely a question of time (11), and similar behavior is expected for all samples with $t < 0.60$.

For reduced samples which were stable at ambient, the temperature for onset of the reoxidation process was established from TGA experiments. Reoxidation starts at 350 K for $t = 0.60$, and the onset temperature increases monotonically up to 540 K for $t = 0.90$. For $t = 1.00$, reoxidation was not detectable by TGA. For all $LaCo_{1-t}Cr_tO_{3-\delta}$ samples, reoxidation was complete at or below 740 K.

3.4. Color

Sample reduction is accompanied by changes in color. In all cases, the color of the reduced samples was lighter and greener than that of their as-prepared counterparts. $LaCoO_{2.5}$ is dark green, but immediately turns black upon reoxidation in air, probably due to $LaCoO_3$ being formed at the surface (Section 4.4). For $t = 0.20$, the reduced state is dark brown with a tint of green after exposure to air. With increasing t throughout the series, the color gradually turned lighter and greener until the sample was close to olive for $t = 0.95$. For $t = 1.00$, the light green color was clearer and less yellow after reduction. After storage at ambient for several months, the originally reduced samples with $0.00 \leq t \leq 0.50$ were black, whereas the more chromium-rich samples were seemingly unchanged. After reoxidation in air at a maximum temperature of 773 K, all samples had regained their original color.

3.5. Unit-Cell Dimensions and Phase Conversions

Unit-cell dimensions for as-prepared, reduced, and reoxidized samples are shown in Fig. 6. For as-prepared samples, the structure data at 298 K are the same as those given in Ref. (8), with purely rhombohedral (R) samples for $t \leq 0.75$, purely orthorhombic (O) for $t \geq 0.85$, and two-phase ($R + O$) samples between these limits. After TPR and subsequent TG reoxidation at 773 K, all samples regained their original structure type and unit-cell dimensions. This also pertains to the sample with $t = 0.80$, which is in the two-phase region at room temperature.

Sample reduction yields a variety of deformed, perovskite-related structures. The main feature for all samples

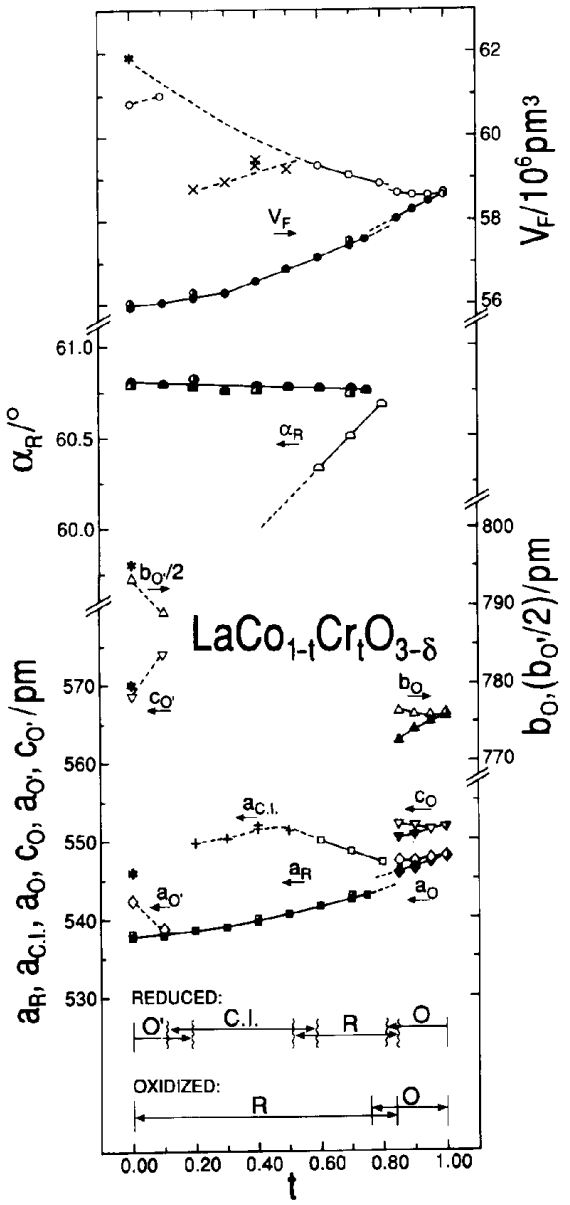

FIG. 6. Unit-cell dimensions of $LaCo_{1-t}Cr_tO_{3-\delta}$ for $0.00 \le t \le 1.00$; $\delta \le 0.500 \cdot (1 - t)$. Structures are denoted O' for orthorhombic brownmillerite-like, R for rhombohedral, and O for orthorhombic perovskite type. C.I. refers to cubic indexing. Filled symbols are used for as-prepared, open for reduced, and half filled for reoxidized samples. Cubic indexed samples are marked by + and ×, while * refers to data quoted from Ref. (4). Calculated errors do not exceed the symbol size, except for the O' samples, where the error is about twice the size of symbols, and for the C.I. samples, where the estimated error is about three times the symbol size (see Sec. 3.5).

is an increase in unit-cell dimensions upon reduction. Samples with $t \le 0.50$ are partially reoxidized at room temperature, and the present structure assignment does not necessarily represent the structure of the fully reduced samples. For all partially reoxidized samples, the Bragg reflections were rather broad. This probably reflects poor crystallinity and/or inhomogeneities in the oxygen distribution.

For $t = 0.00$, the partially reoxidized sample, of average composition $LaCoO_{2.69}$, contained two phases, $LaCoO_3$ and a phase which could be indexed as an orthorhombic (O'), brownmillerite-type structure, except for one weak reflection. The unit-cell dimensions for the latter phase are compared with those reported for $LaCoO_{2.5}$ (4) in Fig. 6. The $LaCoO_3$ phase had sharp reflections and unit-cell dimensions equal to those for the as-prepared sample, indicating a composition close to stoichiometric. For $t = 0.10$, a brownmillerite-like phase similar to that in $LaCoO_{2.69}$ was found. However, three reflections were not indexable on the brownmillerite-type unit cell.

In the region $0.20 \le t \le 0.50$ another structure occurs. There is a systematic change in the positions and splittings of the reflections on going from the brownmillerite-like variant, through this region, and on to the rhombohedral perovskite-like structure. For $t = 0.20$, the characteristic reflection at ~790 pm in the brownmillerite-type structure is absent, indicating that the perovskite-derived unit cell is no longer quadrupled in the b direction. Owing to the few, weak, and diffuse reflections, the actual structure of these samples could not be determined, and cubic indexing was applied, using a consistent set of reflections throughout the region. Support for this choice of indexing is gained from the observed variation of the rhombohedral angle, α_R, with t (Fig. 6). Extrapolation from the rhombohedral region suggests conversion to a cubic structure ($\alpha_R = 60°$) at $t \approx 0.40$. At $t = 0.50$, it still appears possible to index the diffraction pattern on the basis of a rhombohedral unit cell, while for $t = 0.40$, the rhombohedral splitting of the reflections is not detectable. For both compositions, an additional reflection at $d \approx 270$ pm is observed.

The error involved when applying cubic indexing (C.I.) was estimated by comparing the volume per formula unit (V_F) obtained through C.I. with that obtained by the relevant correct indexing for $0.00 \le t \le 0.80$. On this basis, the maximum relative error in V_F for samples with $0.20 \le t \le 0.50$ is estimated to be $\pm 0.3 \cdot 10^6$ pm^3, or about 0.5%.

The samples in question are partially reoxidized, and they probably, like $LaCoO_{2.69}$, consist of two or more phases. However, the present PXD data do not allow further elaboration on this point, and the results for $0.20 \le t \le 0.50$ are labelled C.I. in Fig. 6. The structural regions denoted O', C.I., and R in Fig. 6 may be separated by narrow two-phase regions as indicated in the figure.

Samples with $t \ge 0.60$ are stable in the reduced form at ambient conditions. The difference between the unit-cell dimensions for the reduced and oxidized samples increase with increasing oxygen deficiency (increasing δ, decreasing t). In the region $0.60 \le t \le 0.80$, the structure of the reduced samples is rhombohedral, and the deviation

from cubic symmetry increases with increasing t. Samples with $t \geq 0.85$ are orthorhombic. Within the domain $0.80 < t < 0.85$, a two-phase region must exist because the R to O transition is of first order. The limits marked in Fig. 6 represent the maximum extension of this two-phase region.

3.6. XPS Examination

The (deconvoluted) XPS peaks for La, Co, and O are slightly shifted towards higher binding energies with increasing t, while the chromium peaks remain at the same position for all samples. Neither sample reduction nor sputtering gave rise to significant shifts for any of the samples. Average peak positions are O_I, 528.9; O_{II}, 530.9; O_{III}, 532.9; La_I, 834.1; La_{II}, 837.7; Co_I, 780.1; Co_{II}, 782.5; Cr_I, 575.9; and Cr_{II}, 579.2 eV.

The assessed (integrated and normalized) concentrations of the different species in the samples of $LaCo_{1-t}Cr_tO_3$ are given in Fig. 7. The inset shows the nominal concentrations of La, Co, Cr, and O. As is seen from Fig. 7, the experimentally determined atomic concentrations deviate somewhat from these values.

The total concentration of oxygen, found as the sum of the contributions from the three oxygen peaks, fluctuates around 65 at.%. Inspection of the individual (deconvoluted) oxygen XPS peaks shows that the intensity of the O_I peak increases monotonically on going from $LaCoO_3$ to $LaCrO_3$. The contributions from the O_{II} and O_{III} peaks are added, as they to a certain extent vary at the expense of each other. As seen from Fig. 7, the total concentration of these latter species decreases with increasing t. The total La concentration is constant, around 22 at.% for $t \geq 0.20$. The ~4 at.% higher total La concentration found for $t = 0.00$ is connected with a larger contribution from La_{II} and could reflect "missing" Cr_{II}, *vide infra*.

In the cobalt spectrum, an increase in the intensity of Co_I is accompanied by a decrease in that of Co_{II}. The sum of these cobalt signals, Co_{TOTAL} in Fig. 7, decreases linearly with t, and extrapolates nearly to zero for $LaCrO_3$. For chromium, however, a larger deviation from the expected variation is found. This involves a larger spread in the data points for Cr_{TOTAL} than found for Co_{TOTAL}. Furthermore, the linear (least-squares) fit to the Cr_{TOTAL} data points fails to extrapolate to zero for $LaCoO_3$. Inspection of the individual peaks (Fig. 7) shows that the intensity of Cr_I (at 576 eV) increases linearly with t. The concentration of Cr_I in $LaCrO_3$ equals that of Co_{TOTAL} in $LaCoO_3$, and the linear fits to Co_{TOTAL} and Cr_I concentrations are symmetrical around $t = 0.50$. The concentration of the species represented by the Cr_{II} peak (at 579 eV) fluctuates around some 4 at.%, and this is the source of the scatter in the experimental points for Cr_{TOTAL} and of the nonzero extrapolation; see Fig. 7. The absence

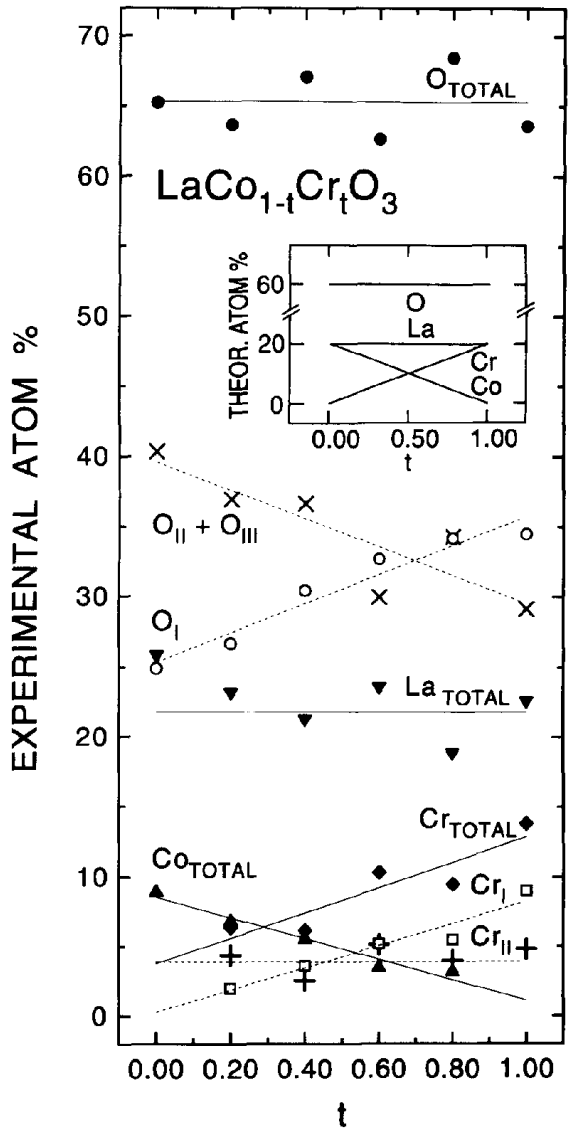

FIG. 7. Concentration dependencies for $LaCo_{1-t}Cr_tO_{3-\delta}$ species analyzed by XPS. Inset shows the corresponding theoretical relationships according to the nominal composition of the samples.

of Cr (notably Cr_{II}) for $t = 0.00$ seems to be "compensated" for by an enhanced La_{II} signal.

After sample reduction, the intensity of Cr_{II} is significantly lowered, both for $t = 1.00$ and 0.80; see Fig. 8 and its inset. The same effect is introduced by sputtering of the as-prepared $LaCrO_3$ sample. In the O 1*s* spectra for $LaCrO_3$, the intensity of O_{II} (at 231 eV) is diminished upon sputtering, whereas the peak profile is more or less unaltered after reduction and storage at ambient conditions. In this respect, the oxygen spectrum for the sample with $t = 0.80$ is quite different. After reduction and storage, the intensity of the O_{III} peak is strongly enhanced for $t = 0.80$. This occurs largely at the expense of O_{II};

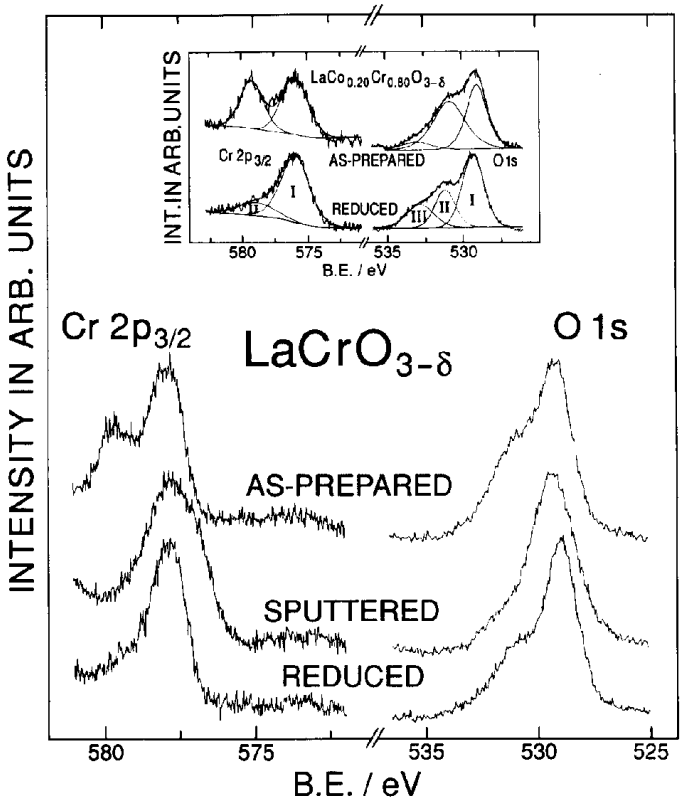

FIG. 8. Intensity of Cr $2p_{3/2}$ and O 1*s* peaks for as-prepared, sputtered, and reduced $LaCo_{1-t}Cr_tO_{3-\delta}$ with $t = 0.80$ (inset) and 1.00. Inset gives the deconvolution of the oxygen peaks in O_I, O_{II}, and O_{III}, and the chromium peaks in Cr_I and Cr_{II}.

see the inset to Fig. 8. Due to the stability problems for the reduced samples with $t < 0.60$, these were not examined by XPS.

4. DISCUSSION

4.1. XPS Data

The partially overlapping peaks in the spectra of lanthanum, cobalt, chromium, and oxygen have different origins. The La peak at 837.7 eV (La_{II}) is a satellite to the 834.1 (La_I) $3d_{5/2}$ peak, and is due to charge-transfer from a neighboring oxygen ion to the empty 4*f* shell of lanthanum (12). Thus, the two La peaks do not reflect different La species, and the enhanced intensity of the La_{II} peak for $LaCoO_3$ signalizes a difference in the charge-transfer process for this sample compared to the chromium-substituted samples.

In the case of the cobalt spectrum, the $2p_{3/2}$ peak is here deconvoluted into two peaks. The main feature, at 780.1 eV (Co_I), reflects Co^{III} (high and low spin) (13). The weak peak introduced at higher binding energy has to our knowledge not been reported previously. In any case, the total $2p_{3/2}$ peak profile does not deviate much (perhaps only insignificantly) from experimental peak profiles reported in the literature (13–15).

The chromium spectrum is also separated into two peaks, Cr_I at 575.9 eV and Cr_{II} at 579.2 eV. The first peak is unequivocally assigned to Cr^{III} (14, 16). The Cr_{II} peak is assigned to a higher valent chromium state, perhaps Cr^V or Cr^{VI}, here denoted Cr^{HV}. XPS peaks for the latter species are reported at 578.8 eV for Cr^V in $LaCrO_4$ (16) and from 578.9 to 579.8 eV for compounds containing Cr^{VI} (17).

The interpretation of the oxygen spectra for perovskite-type oxides has been a source of some dispute. The peak at about 529 eV (O_I) is attributed to a normal O 1*s* (O^{2-}) signal, while the controversy is connected with the peak at some 531 eV (O_{II}). Rao and Sarma (18) studied the O 1*s* core level spectra of $LaMO_3$ (M = V, Cr, Mn, Fe, Co, and Ni) and found a systematic variation in the intensity of this peak. They therefore concluded that the 531 eV peak reflects an intrinsic feature of $LaMO_3$. Experiments performed by Fierro and Tejuca (19) showed the same systematics in the peak intensity throughout the $LaMO_3$ series, but in addition they found that the relative intensity of the 531 eV peak was decreased when the temperature during the sample pretreatment was increased. The latter authors assigned this peak to adsorbed oxygen (presumably in the form of O^-), in agreement with previous assignments for oxygen adsorbed on $LaCoO_3$ by Ichimura *et al.* (15) and on $La_{1-x}Sr_xCoO_3$ by Yamazoe *et al.* (20). The interpretation of the peak at 533 eV (O_{III}) is even more uncertain. It should be noted that the peak is seldom observed [apparently absent in Refs. (18–20), but found in Ref. (21)]. Furthermore, B. E. for oxygen in water is tabulated as 533.1 eV (22). The present samples were stored under ambient conditions prior to the XPS measurements and the 533 eV peak is therefore likely to reflect chemisorbed water (perhaps converted to OH^-) on the sample surface.

A general trend for the atomic concentrations deduced from the XPS data is that the total contents of oxygen, lanthanum, and cobalt are in good to reasonable accord with the variations in the nominal sample composition. Chromium, however, is found in excess. Since the concentration of Cr^{HV} decreases after sample reduction and sputtering, it is suggested that these species occur only at the sample surfaces, in particular since the Cr^{III} concentration varies in general accordance with the nominal composition of the samples.

Although the total oxygen content in the surface of the $LaCo_{1-t}Cr_tO_3$ samples is constant, variations are found with respect to the distribution between bulk O^{2-} and surface oxygen species (O^- and possibly OH^-). The relative amount of surface oxygen (O_{II} plus O_{III}) decreases on going from $LaCoO_3$ to $LaCrO_3$, in accord with the

findings for $LaMO_3$ (18, 19). This decrease is compensated for by an increase in the bulk (O_I) oxygen content, perhaps a manifestation of a decreased ability to form oxygen vacancies at the surface, where oxygen and water can adsorb. Further support for this suggestion is found in the O 1*s* spectra in Fig. 8, where sputtering of $LaCrO_3$ is seen to decrease the content of surface oxygen. In the case of the $t = 0.80$ sample, reduction can either have generated oxygen vacancies, which are occupied by water or OH^- upon the subsequent exposure to ambient, or have left OH^- on the surface after the treatment with H_2. For $LaCrO_3$, reduction seems only to influence the content of Cr^{HV}, while the oxygen species are maintained more or less unaltered (at least after exposure to ambient conditions).

4.2. *Oxygen Stoichiometry and Sample Reduction*

After the final calcination and slow cooling to room temperature, $LaCoO_{3-\delta}$ is expected to be stoichiometric [viz. $\delta = 0.00$, according to earlier findings for comparable samples investigated by TGA (23–25), which is the best method for measuring the oxygen stoichiometry of this perovskite-type oxide (26)]. For $LaCrO_3$, oxygen nonstoichiometry has not previously been detected (25, 27), but slight oxygen excess at low temperatures has been suggested (28). It is reasonable to postulate oxygen stoichiometry, $\delta = 0.00$, for all as-prepared samples.

The sample reduction process is fundamentally different in $LaCoO_3$ and $LaCrO_3$. Within the experimental error, the reduction of $LaCoO_3$ below ~750 K proceeds until all cobalt is reduced to Co^{II}. This is in accord with earlier reports that $LaCoO_3$ is reduced to $LaCoO_{2.5}$ by H_2 (1, 4, 24) or by CO (29).

It is tempting to suggest that the dual peak profile for the bulk reduction of $LaCoO_3$ (Fig. 2) corresponds to the formation of an intermediate structure $LaCoO_{2.75}$. This composition corresponds to $n = 4$ in the suggested homologous series $A_nB_nO_{3n-1}$ (4, 5). An analogous nickel phase, $La_4Ni_4O_{11}$, has recently been isolated by annealing in an H_2/He gas mixture at 415 K (3). The regular TPR (temperature scan) technique is not expected to suffice for isolating such an intermediate for $La_nCo_nO_{3n-1}$, as the TPR peak separation (see Sec. 3.2) remained virtually unaltered when the heating rate was decreased from 5 to 1 K min^{-1}.

On the basis of the reported stability and stoichiometric nature of $LaCrO_3$, the observation of a slight sample reduction was at first sight surprising. However, similar behavior has previously been observed for $LaCrO_3$ and explained as reduction of surface Cr^{III} to Cr^{II} (7). The presently observed reduction corresponds to a very small amount of oxygen, 0.0056 mole per mole sample. This amounts to about one surface layer of oxygen, depending on the frequencies of the most commonly exposed surfaces. In our view, this oxygen probably originates from the reduction of Cr^{HV} at the surface (see Sec. 4.1). According to XPS (Sec. 3.6 and Fig. 7), such species compose about $\frac{1}{3}$ of the detected chromium in the as-prepared sample. After TPR or sputtering, the amount of Cr^{HV} is significantly diminished, whereas the amount of Cr^{III} is correspondingly increased. Thus, we suggest that the slight reduction of lanthanum chromite involves conversion of surface Cr^{HV} to Cr^{III}.

Cr^{HV} could be introduced through the presence of lower-valent, solid solution impurities in the samples. However, analyses of the starting materials showed that this explanation was unlikely, in particular since XPS showed no evidence of impurities in the required concentrations.

Another conceivable source of Cr^{HV} is the presence of $LaCrO_4$ in an amount below the detection limit of PXD. However, $LaCrO_4$ decomposes to $LaCrO_3$ at ~1050 K during TGA (30) and some 200 K lower under isothermal conditions (31). The present $LaCrO_3$ samples were heated at 1170 K for 20 hr, and $LaCrO_4$ should thus be eliminated in the as-prepared state. [Regeneration of $LaCrO_4$ may be imagined to take place during the slow cooling of the samples in air, but an attempt to oxidize $LaCrO_3$ to $LaCrO_4$ in air at 723 K for 6 days proved unsuccessful. However, oxygenation to $LaCrO_{4.4}$ has been performed, but under extreme conditions with 130 atm oxygen at 873 K (27).] Another indication of the absence of $LaCrO_4$ is the increase in the temperature of the first reduction peak for high values of *t* (Figs. 2 and 3). If a compound like $LaCrO_4$ were reduced, the process would be expected to take place at a "fixed" temperature.

Having ruled out two possible sources of Cr^{HV}, one arrives at the likely conclusion that the higher valency is a result of oxygen saturation of the surface cation bonds during the cooling of the $LaCrO_3$ samples in air, a process which probably involves surface reconstruction. This could involve diffusion of a slight amount of chromium towards the surface, where it could be bound to oxygen, possibly in a tetrahedral geometry. Sample reduction could involve removal of this oxygen, thus decreasing the amount of Cr^{HV}. Subsequently, local surface reconstruction could take place, while depletion of the "excess" chromium would presumably be kinetically hindered. In this context, it should be recalled that the reduced surface of $LaCrO_3$ appears to be stable at ambient, whereas the characteristics after heating to 773 K in air is compatible with reconstruction and resaturation of surface cation bonds. The processes in question are also observed through the color changes of $LaCrO_3$ upon reduction, storage, and reoxidation.

Assuming oxygen stoichiometry in as-prepared $LaCo_{1-t}Cr_tO_3$, Fig. 4 verifies that the reduction proceeds to

$LaCo_{1-t}Cr_tO_{3-\delta}$, where $\delta = 0.500 \cdot (1 - t)$ which corresponds to reduction of all Co^{III} to Co^{II}. This is in excellent agreement with the findings for $LaCoO_3$ and $LaCrO_3$.

The individual peaks observed by TPR require some comments. The double peak character for $t = 0.20$ may reflect a two-step reduction process similar to that considered for $LaCoO_3$. The splitting of the peak in question becomes less pronounced for $t \geq 0.40$, but the peak as such is found for all samples with $t \leq 0.95$ and in all cases is interpreted as reduction of Co^{III} to Co^{II}.

The additional peak which enters the TPR profiles at lower temperatures for $t \geq 0.40$ is similar to that found for $LaCrO_3$, both with respect to the temperature at which it occurs and the peak profile (perhaps with an exception for $t = 0.60$). The amount of oxygen involved in this low-temperature reduction step is small, and nearly constant for $t \geq 0.80$ (Fig. 4). This peak is therefore assumed to reflect removal of surface oxygen species upon reduction of Cr^{HV} for all samples with $t \geq 0.40$.

Both the high- and low-temperature reduction steps are shifted to higher temperatures with increasing t for $t \geq 0.80$. The reduction at high temperatures is a bulk process, involving Co^{III}, Co^{II}, oxygen, and oxygen vacancies. As the concentration of Co in $LaCo_{1-t}Cr_tO_3$ decreases, the concentration of oxygen vacancies, which controls the oxygen diffusion during the reduction process, decreases. Hence, the diffusion rate from the bulk to the surface decreases, and simple kinetics may shift the reduction process to higher temperatures during TPR experiments.

A similar explanation is suggested for the increased temperature of the low-temperature (surface oxygen) peak with increasing t. In samples which contain both Co and Cr, the surface oxygen species will statistically be involved with ions of both metals. Assuming the same reaction tendency for surface species as for bulk species, oxygen bound to Co should be easier to remove than that bound to Cr. With increasing Cr content, the fraction of oxygen bound to Cr increases, and oxygen removal will consequently require more reductive conditions; in the present case, higher temperature.

4.3. *Structural Properties of the Reduced Phases*

The suggested brownmillerite-type structure for $LaCoO_{2.5}$[$La_2Co_2O_5$ (4)] consists of alternate layers of Co in octahedral and tetrahedral sites (see the schematic representation in Fig. 9B). The structure may be derived from the perovskite-type structure (Fig. 9A) by removing every second row of oxygen atoms from alternate planes. The present unit-cell dimensions (Fig. 6) are somewhat smaller than those reported in the literature (4). This probably originates from differences in oxygen stoichiometry since the present sample was partially reoxidized into a two-phase mixture of $LaCoO_3$ and $La_2Co_2O_y$, where $5 \leq y < 5.38$ (probably close to the lower limit).

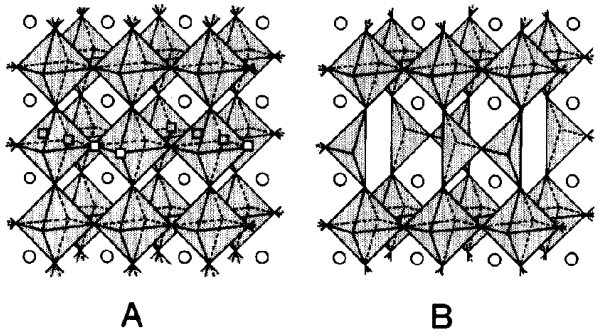

FIG. 9. Schematic comparison of sections of the perovskite- (A) and brownmillerite-type (B) structures in perspective. Oxygen is located at the corners of the coordination octahedra and tetrahedra, and Co/Cr at their centers. La is shown by ○ and oxygen positions in the perovskite-type structure which become vacant in the brownmillerite type are symbolized by □.

The structure for $t = 0.10$ is most probably also based on a brownmillerite-type atomic arrangement. Because $\delta \leq 0.45$ in $LaCo_{0.90}Cr_{0.10}O_{3-\delta}$, the brownmillerite-type phase must be able to accommodate a certain excess of oxygen and still retain the ordered vacancy feature. In the region $0.20 \leq t \leq 0.50$, the unidentified structure occurs.

Samples $0.60 \leq t \leq 1.00$ are stable with respect to reoxidation at ambient, and their structures are of the rhombohedral or orthorhombic perovskite type. Their oxygen content during PXD is specified by $\delta = 0.500 \cdot (1 - t)$. With increasing δ, there is an increase in unit-cell dimensions relative to those of the oxidized samples (Fig. 6). In the present region, one may envisage the reduction mechanism as a consecutive removal of oxygen ions from the structure, where each removal affects two neighboring cobalt ions by leaving them pentacoordinated. In this process, the ionic radius for Co increases from 61 (Co^{III}) to 67 (Co^{II}) pm (32), which in turn contributes to the expansion of the perovskite-type lattice.

4.4. *Reoxidation*

The reoxidation of $LaCo_{1-t}Cr_tO_{3-\delta}$ depends on a complex combination of variables like composition (t), temperature, and time, and sample specifics like degree of crystallinity and particle size.

One may envisage the first, rapid reoxidation of $LaCoO_{2.5}$ at ambient temperature as facilitated by the fast oxygen diffusion allowed by the relatively open brownmillerite-type structure (Fig. 9B). Furthermore, the stabilization energies of perovskite-like structures are large, a few hundred kJ mol^{-1} (33). This could lead to a relative stabilization of the high-valency state Co^{III}, and explain the observed spontaneous nature of the reoxidation reaction. In addition, the reaction from the oxygen-deficient brownmillerite- to the oxygen-saturated perovskite-type

structure is facilitated because little structural reorganization is required.

After an initial, vigorous reoxidation, a layer of $LaCoO_3$ is formed on the sample surface. This layer probably acts as a diffusion barrier and could to some extent hinder further oxidation of the sample. However, the diffusion is only slowed down; given sufficient time, the samples will eventually be fully reoxidized to $LaCoO_3$ (11).

On passing through the solid-solution series from t = 0.00 to 1.00, the temperature required for reoxidation increases. This is coupled to the decreasing number of oxygen vacancies available in the reduced samples with increasing t, which again leads to lowering of the oxygen diffusion rates. Thus, for samples with a low content of Cr, reoxidation can proceed at and below room temperature, whereas reoxidation of the t = 0.90 sample requires 540 K.

$LaCrO_3$ can be brought back to the "as-prepared" state by reoxidation at elevated temperatures. In this case, reduction as well as reoxidation are processes which only involve reconstruction of the sample surface.

ACKNOWLEDGMENTS

The authors express their gratitude to Cand. Scient. Sissel Jørgensen at the Centre for Materials Research for XPS measurements and helpful discussions, and to SINTEF, Oslo, for placing the TPR equipment at their disposal. The financial support of the Norwegian Research Council (NFR) is gratefully acknowledged.

REFERENCES

1. M. Crespin and W. K. Hall, *J. Catal.* **69,** 359 (1981).
2. M. Crespin, P. Levitz, and L. Gatineau, *J. Chem. Soc., Faraday Trans.* **79,** 1181 (1983).
3. M. J. Sayagués, M. Vallet-Regí, A. Caneiro, and J. M. González-Calbet, *J. Solid State Chem.* **110,** 295 (1994).
4. K. Vidyasagar, A. Reller, J. Gopalakrishnan, and C. N. R. Rao, *J. Chem. Soc., Chem. Commun.* 7 (1985).
5. M. T. Anderson, J. T. Vaughey, and K. R. Poeppelmeier, *Chem. Mater.* **5,** 151 (1993).
6. T. Nakamura, G. Petzow, and L. J. Gauckler, *Mater. Res. Bull.* **14,** 649 (1979).
7. J. L. G. Fierro and L. G. Tejuca, *J. Catal.* **87,** 126 (1984).
8. B. Gilbu, H. Fjellvåg, and A. Kjekshus, *Acta Chem. Scand.* **48,** 37 (1994).
9. N. O. Ersson, Program CELLKANT, Chemical Institute, University of Uppsala, Sweden, 1981.
10. Kratos Analytical, Data Sheet (reprinted 1992).
11. O. H. Hansteen, Thesis, University of Oslo (1994).
12. C. K. Jørgensen and H. Berthou, *Chem. Phys. Lett.* **13,** 186 (1972).
13. I. G. Main, G. A. Robins, and G. Demazeau, *J. Phys. C: Solid State Phys.* **14,** 3633 (1981).
14. D. J. Lam, B. W. Veal, and D. E. Ellis, *Phys. Rev. B: Condens. Matter* **22,** 5730 (1980).
15. K. Ichimura, Y. Inoue, and I. Yasumori, *Bull. Chem. Soc. Jpn.* **53,** 3044 (1980).
16. H. Konno, H. Tachikawa, A. Furusaki, and R. Furuichi, *Anal. Sci.* **8,** 641 (1992).
17. G. C. Allen and P. M. Tucker, *Inorg. Chim. Acta* **16,** 41 (1976).
18. G. R. Rao and D. D. Sarma, *Mod. Phys. Lett. B* **4,** 277 (1990).
19. J. L. G. Fierro and L. G. Tejuca, *Appl. Surf. Sci.* **27,** 453 (1987).
20. N. Yamazoe, Y. Teraoka, and T. Seiyama, *Chem. Lett.* 1767 (1981).
21. D. K. Chakrabarty, D. Y. Rao, and P. D. Prabhawalkar, *React. Kinet. Catal. Lett.* **31,** 413 (1986).
22. C. D. Wagner, *in* "Practical Surface Analysis by Auger and X-Ray Photoelectron Spectroscopy" (D. Briggs and M. P. Seah, Eds.), 2nd ed., Vol. 1, Appendix 5. (1990).
23. J. Mizusaki, Y. Mima, S. Yamauchi, K. Fueki, and H. Tagawa, *J. Solid State Chem.* **80,** 102 (1989).
24. I.-H. Park and H.-P. Lee, *Bull. Korean Chem. Soc.* **9,** 283 (1988).
25. L. Wachowski, *Z. Phys. Chem. (Leipzig)* **269,** 743 (1988).
26. K. Woxholt, Thesis, University of Oslo (1994).
27. B. C. Tofield and W. R. Scott, *J. Solid State Chem.* **10,** 183 (1974).
28. R. J. H. Voorhoeve, J. P. Remeika, and L. E. Trimble, *Ann. N.Y. Acad. Sci.* **272,** 3 (1976).
29. K. S. Chan, J. Ma, S. Jaenicke, G. K. Chuah, and J. Y. Lee, *Appl. Catal. A* **107,** 201 (1994).
30. A. Roy and K. Nag, *J. Inorg. Nucl. Chem.* **40,** 1501 (1978).
31. P. S. Devi and M. S. Rao, *Thermochim. Acta* **15,** 181 (1989).
32. R. D. Shannon, *Acta Crystallogr. Sec. A* **32,** 751 (1976).
33. L. D. Finkel'shtein, G. V. Bazuev, N. D. Samsonova, and S. A. Nemnonov, *Zh. Neorg. Khim.* **24,** 2609 (1979); Engl. transl., *Russ. J. Inorg. Chem.* **24,** 1448 (1979).